Effect of stress-induced magnetization on crack monitoring by self magnetic flux leakage method

van der Horst, Menno; van Kreveld, Sylvia; Kaminski, Mirek

DOI
10.3233/JAE-180031

Publication date
2019

Document Version
Accepted author manuscript

Published in
International Journal of Applied Electromagnetics and Mechanics

Effect of Stress-Induced Magnetization on Crack Monitoring by Self Magnetic Flux Leakage Method

Menno Patrick van der Horst [a]
Sylvia Lyanne van Kreveld [a]
Miroslaw Lech Kaminski [a]

[a] Delft University of Technology
Mekelweg 2
2628 CD Delft
The Netherlands
menno_vd_horst@hotmail.com
s.l.vankreveld@student.tudelft.nl
m.l.kaminski@tudelft.nl

Abstract

Wireless crack monitoring on ships and offshore structures based on Self Magnetic Flux Leakage (SMFL) measurements is a promising method to guarantee the structural integrity in a more effective way, leading to reduced operational costs and increased safety. For accurate crack sizing, the SMFL measurements must be interpreted correctly, also during cyclic loading. Not much research has been done that focus on the effect of high cyclic stresses on the magnetization of ferromagnetic steels in weak magnetic fields. The aim of the research presented in this paper is to investigate the effect of stress-induced magnetization on the SMFL in the stress concentration zone of a structural steel plate, and its implications for crack monitoring by the SMFL method. By means of an experiment, measured stress magnetization curves were obtained in a grid of points around an elliptical hole in a steel plate that was cyclically loaded up to the yield stress. The results show that the stress-induced magnetization causes a maximum variation of the measured signal of 25 μT, which is fully reversible. It is concluded that, depending on the application, this stress-induced variation may need to be taken into account for the interpretation of the measured signals by a crack monitoring system using the SMFL method.

Keywords

Crack monitoring; Self Magnetic Flux Leakage; stress magnetization; ferromagnetic steel; cyclic loading.

1. Introduction

Structural health monitoring has become an attractive concept as sensors have become much more affordable and because of the progress made in handling large amounts of data. Many non-destructive evaluation methods have emerged during the last decades that can aid in detection of structural damage such as fatigue or corrosion. Still, the majority of inspections for ship and offshore structures are done visually by surveyors. A detected crack of an acceptable size for safe operation must be followed up during successive inspections. Instead of additional inspection by surveyors, a wireless crack monitoring system is proposed in [1] that is based on Self Magnetic Flux Leakage (SMFL) measurements and warns the operator when the crack has reached its predefined unacceptable size. Such a system could guarantee the structural integrity of ship and offshore structures in a more effective way, leading to reduced operational costs and increased safety.

For accurate sizing of the crack, SMFL measurements must be interpreted correctly. Earlier research gave insight in the contributions of Earth-induced magnetization and permanent magnetization to the SMFL signals near a crack in a structural steel plate that is unloaded [2, 3]. When applying fatigue loads on a cracked specimen, the SMFL will change due to crack opening [4] and stress-induced magnetization. Much research has been done on stress-induced magnetization, which is caused by the magnetomechanical effect [5–11]. However, most studies focus on the effect of small and static stresses for large applied fields. For passive magnetic crack monitoring, on the other hand, it is important to study and quantify the effect of large and cyclic stresses in weak magnetic fields. Therefore, the objective of the research presented in this paper is to investigate the effect of stress-induced magnetization on the SMFL in the stress concentration zone of a structural steel plate, and its implications for crack monitoring by the SMFL method.

An experimental method to measure the effect of stress-induced magnetization on the SMFL is described in the next section and the experimental results are presented in section 3. The Earth-induced magnetization and the stress distribution for the experimental specimen are numerically simulated by the Finite Element Method in section 4. This section also presents a theoretical framework to simulate the stress-induced magnetization for a qualitative comparison with the experimental results. Finally, all the results are discussed in section 5 and the conclusions are presented in section 6.

2. Method

2.1 Test specimen

An FeE235 structural steel plate is used as test specimen for the conducted experiment. The plate has a width of 70 mm and a thickness of 5 mm and has an elliptical hole in the middle of 10 by 3 mm, see Fig. 1. The dimensions of the defect are chosen such that it creates a significant stress concentration zone while having a large enough width so that the opening of the hole caused by applied tension is negligible. The length of the specimen is sufficient to clamp it in the MTS fatigue testing machine, see Fig. 2, and have sufficient length left to ensure a uniform stress distribution in the middle of the plate. The MTS fatigue testing machine can apply loads in axial direction of up to 350 kN with a frequency of up to 20 Hz.

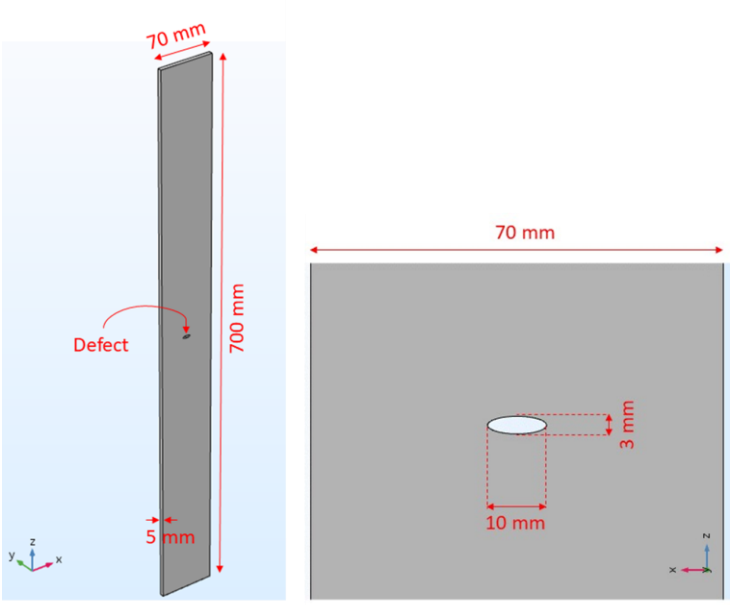

Fig. 1 FeE235 steel specimen with dimensions.

Fig. 2 Specimen while clamped in the MTS fatigue testing machine.

2.2 Experiment 1

The fatigue machine is programmed to apply a linearly increasing load from 0 kN to 82.25 kN in 40 seconds that then decreases again to 0 kN with the same rate. This load cycle is repeated two more times resulting in the force-time diagram shown in Fig. 3. A tensile load of 82.25 kN results in a far field stress of 235 MPa, which makes it the maximum load before the specimen could start to yield.

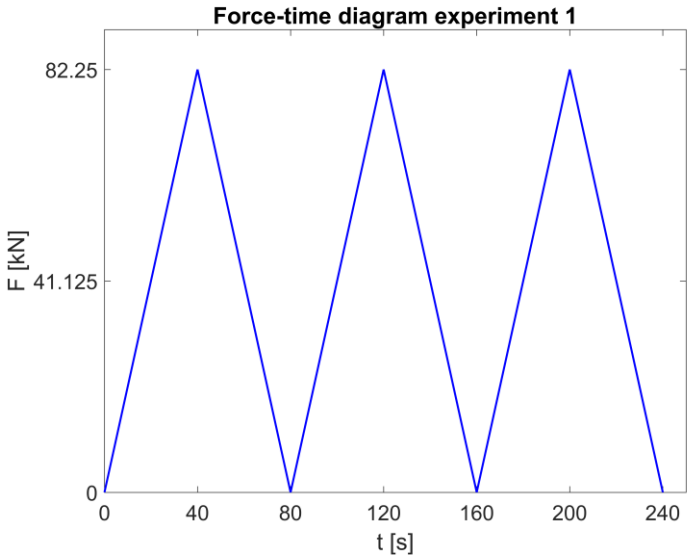

Fig. 3 Load path experiment 1.

While the specimen is loaded, magnetic measurements are taken near the plate surface using a single axis magnetometer with 1 µT sensitivity [12] in out-of-plane direction, which is the y-direction in this case, see Fig. 4. The Hall probe of the magnetometer is kept at a constant altitude of 1 mm from the plate surface and takes measurements with a sampling rate of 5 Hz. These continuous measurement cycles are repeated in a grid of 14 locations around the elliptical hole as shown in Fig. 5.

Fig. 4 Setup for magnetic measurements experiment 1.

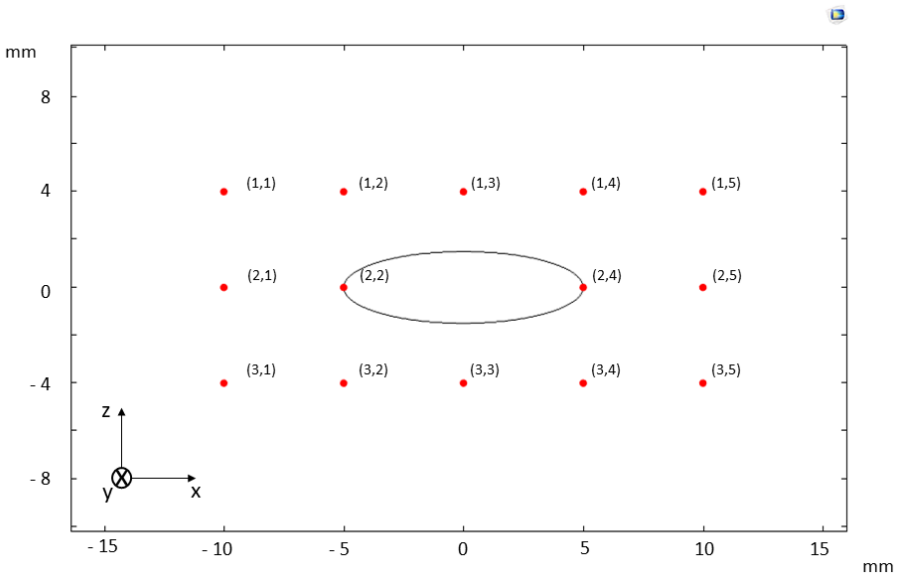

Fig. 5 Measurement grid around elliptical hole.

2.3 Experiment 2

To investigate whether local plasticity plays a role in experiment 1, a similar experiment is conducted where measurements are taken in the elastic region away from the elliptical hole. The same test specimen is used but with an extra row of five measurement points 50 mm above the elliptical hole, see Fig. 6. The points are numbered from left to right as (0, 1) to (0, 5).

Fig. 6 Test specimen with extra row of five measurement points 50 mm above elliptical hole.

The same load path is applied but with a minimum load of 3 kN to avoid any overshoot into compressive forces that could lead to unwanted bending stresses and a maximum load of 77 kN to

be certain that no plasticity occurs around the extra row of measurement points. The force-time diagram of experiment 2 can be seen in Fig. 7.

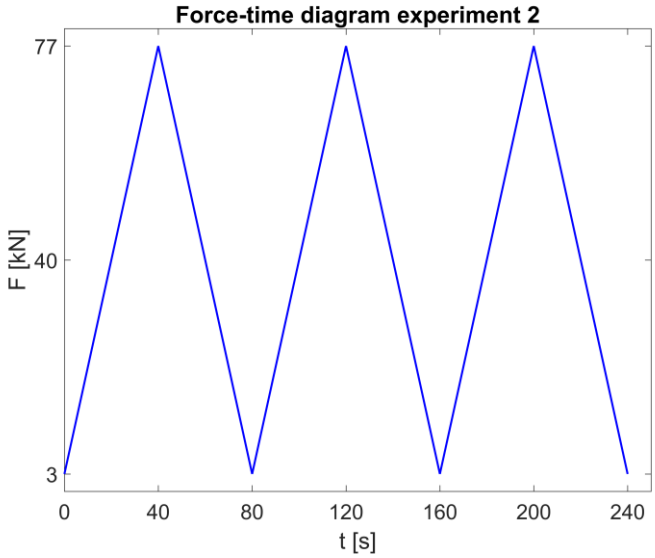

Fig. 7 Load path experiment 2.

The same setup is used with the single axis magnetometer taking measurements in y-direction with a sampling rate of 5 Hz at the five measurement points consecutively and with an altitude of 1 mm from the plate surface, see Fig. 8.

Fig. 8 Setup for magnetic measurements experiment 2.

3. Experimental Results

3.1 Results Experiment 1

Before starting the experiment, the background field was measured. The resulting background field in x, y and z-direction can be found in Table 1.

Direction	B [µT]
x	-10
y	-11
z	-20

Table 1: Background field before experiment 1.

The measured time traces of the magnetic flux density in y-direction are shown in Fig. 9. The chart on the left shows the time traces for row 1 of the measurement grid, the middle chart for row 2 and the chart on the right for row 3.

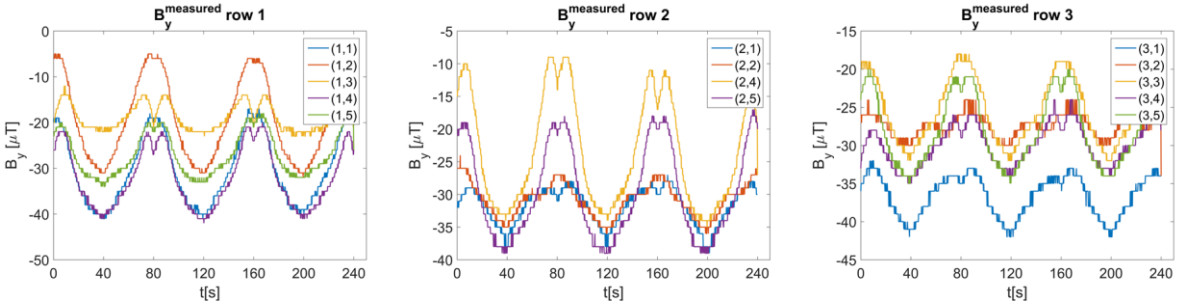

Fig. 9 Raw measurement data experiment 1.

The measured magnetic flux density is a summation of background field, Earth-induced field, permanent field and stress-induced field, so it reads

$$B_y^{measured} = B_y^{BG} + B_y^{ind} + B_y^{per} + B_y^{\sigma} . \tag{3.1}$$

The background field, Earth-induced field, and permanent field are assumed to be constant in time during loading as changes in environment, plate geometry and magnetic material properties, and coupling between stress-induced magnetization and permanent magnetization are assumed negligible. Therefore, the only change in magnetic flux density during loading is attributed to the stress-induced magnetic flux density. The stress-induced magnetic flux density can then be calculated by subtracting the measured magnetic flux density at t=0 from the entire time series as follows:

$$B_y^{\sigma}(t) = B_y^{measured}(t) - B_y^{measured}(t=0) . \tag{3.2}$$

The resulting time traces for the stress-induced magnetic flux density in y-direction are shown in Fig. 10. Note that a moving average filter with a span of 15 data points (i.e. 3 s) is applied on the raw data to reduce perturbations due to the discrete sensor output.

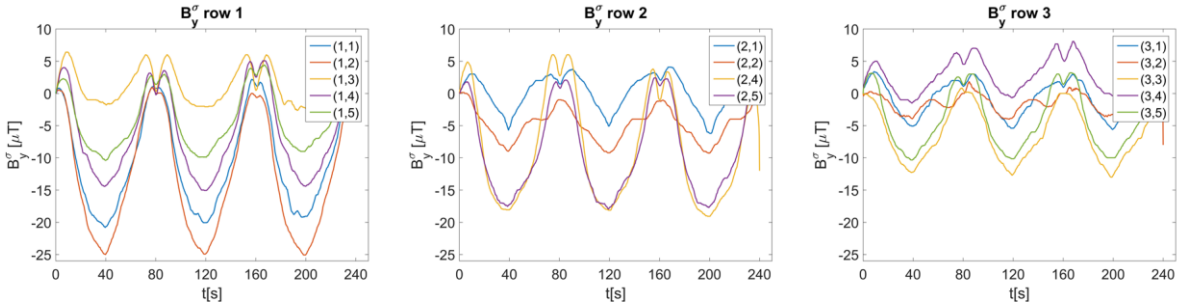

Fig. 10 Moving average filtered stress-induced magnetic flux density in y-direction rows 1-3.

The three load cycles can be subdivided into six periods: three periods with increasing load and three periods with decreasing load. In Fig. 11, the results for these six periods are plotted as function of the applied load for point (1, 2), which showed the highest maximum stress-induced magnetic flux density. The beginning and end of all curves coincide with each other but the path in between is different for periods with increasing load than for periods with decreasing load. Figs. 12-14 show the average curves for periods 1, 3 and 5 as “Increasing F” and for periods 2, 4 and 6 as “Decreasing F” for rows 1, 2 and 3 respectively. In each measurement point, a small difference can be observed in the stress-induced magnetization curve for increasing load versus decreasing load. Most importantly, the stress-induced magnetization increases with increasing load in each measurement point but the magnitude varies between measurement points.

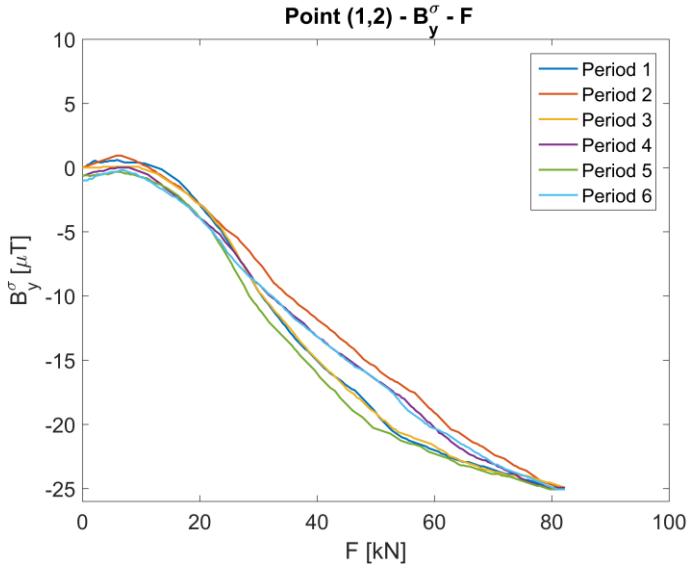

Fig. 11 Stress-induced B_y versus applied load for point (1, 2).

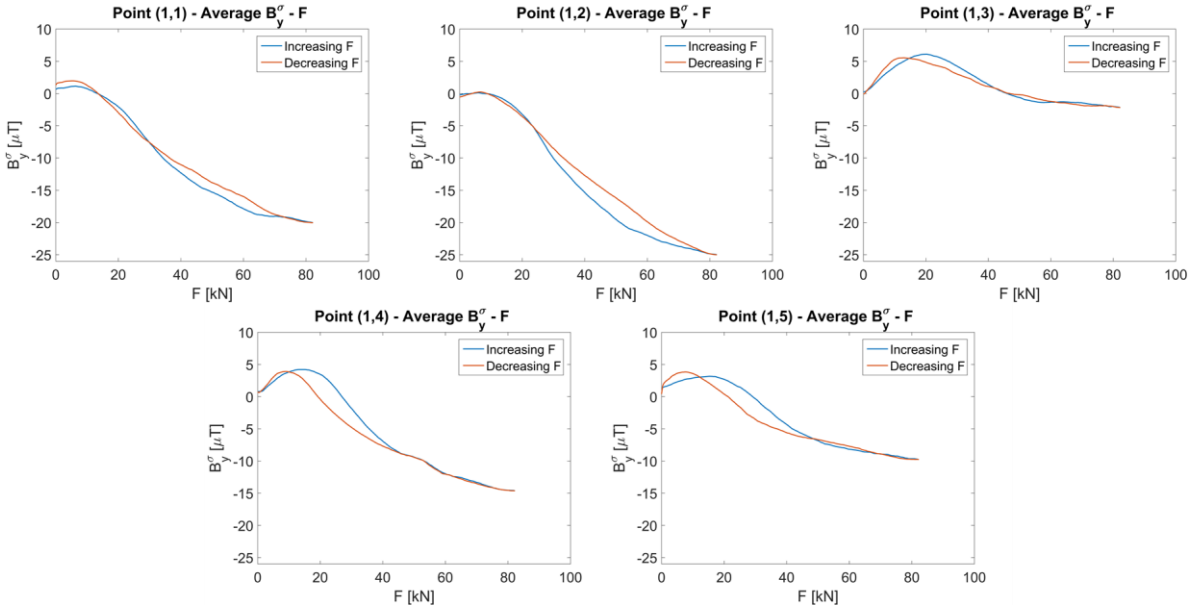

Fig. 12 Averaged stress-induced B_y versus applied load for row 1.

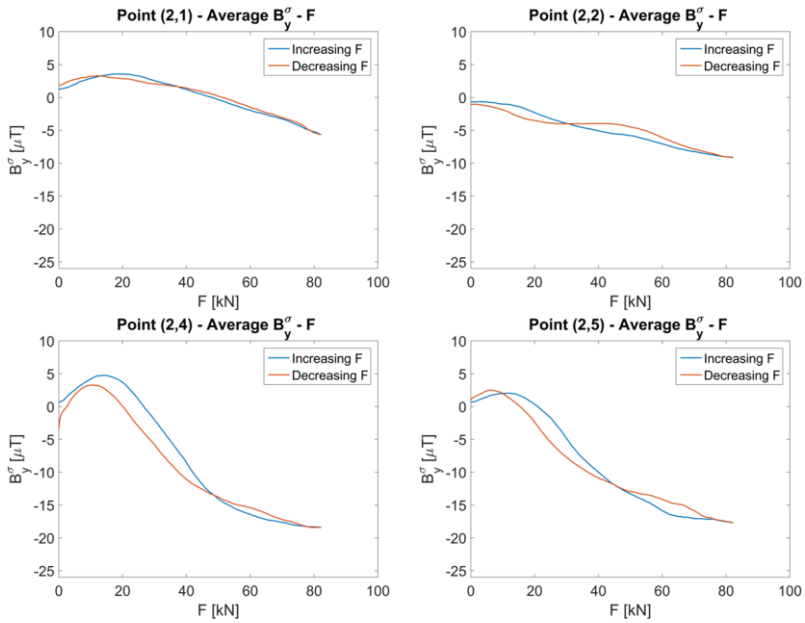

Fig. 13 Averaged stress-induced B_y versus applied load for row 2.

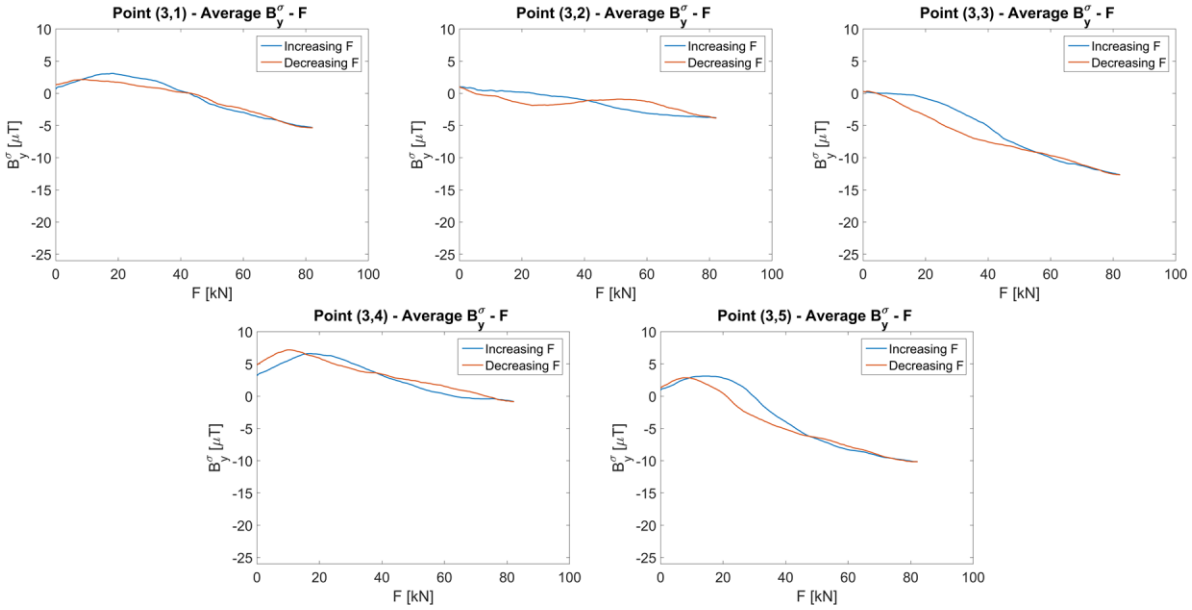

Fig. 14 Averaged stress-induced B_y versus applied load for row 3.

3.2 Results Experiment 2

Experiment 2 was conducted a week after experiment 1, so the background field was measured again. The resulting background field in x, y and z-direction can be found in Table 2.

Direction	B [μT]
x	-5
y	-14
z	-18

Table 2: Background field before experiment 2.

Post-processing of the measured data for experiment 2 is done in the same manner as for experiment 1. The measured time traces of the magnetic flux density in y-direction are shown in Fig. 15 and those for the stress-induced magnetic flux density in y-direction, calculated according to equation (3.2), are shown in Fig. 16. Again, a moving average filter with a span of 15 is applied to the raw data to obtain smooth curves in Fig. 16. The average stress-induced magnetic flux density in y-direction for increasing load and decreasing load is plotted against the applied load in Fig. 17 for all five measurement points in row 0.

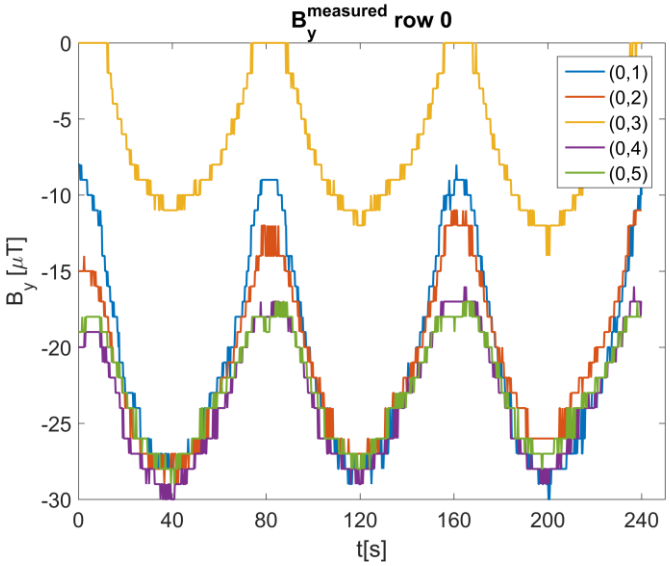

Fig. 15 Raw measurement data experiment 2.

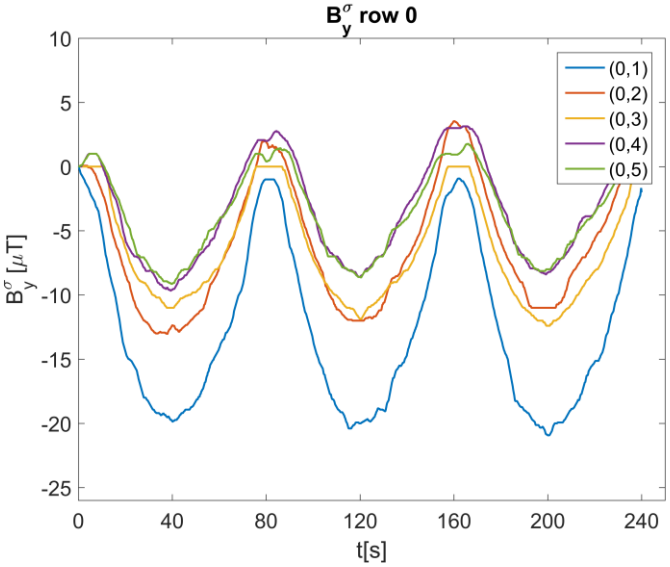

Fig. 16 Moving average filtered stress-induced magnetic flux density in y-direction row 0.

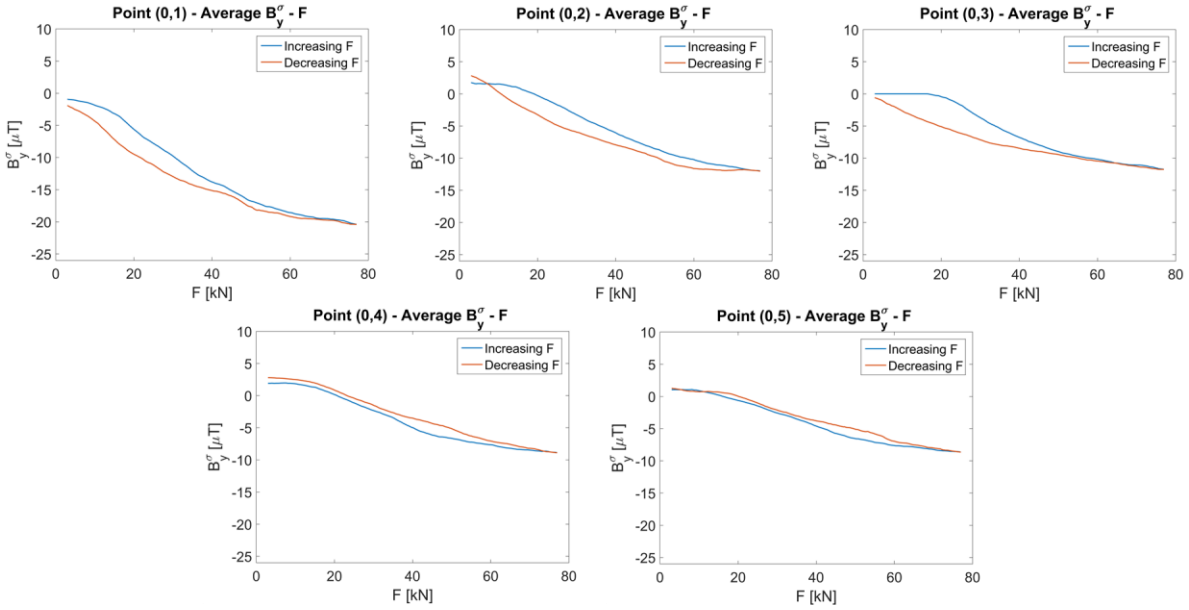

Fig. 17 Averaged stress-induced B_y versus applied load for row 0.

4. Numerical Simulation

4.1 Magnetic FE Model

The Earth-induced magnetization from equation (3.1) can be modeled reasonably accurate with a linear magneto-static Finite Element model using the software package COMSOL Multiphysics. The same steel is used as in [3] so the material is modeled linearly with a relative permeability of 225. The geometry from Fig. 1 is modeled with a vacuum box of 15x15x15 m around the plate as model domain. On the domain edges, boundary conditions are applied such that a homogeneous background field is generated with the measured values from Table 1. The model is meshed using tetrahedral elements and results are obtained in the plane around the elliptical hole and at an altitude of 1 mm from the plate surface where the measurements were taken. The results for the magnetic flux density in y-direction are shown in Fig. 18 together with the measurement grid. Note that this model only considers the induced magnetization caused by the background field in combination with the plate's ferromagnetic properties.

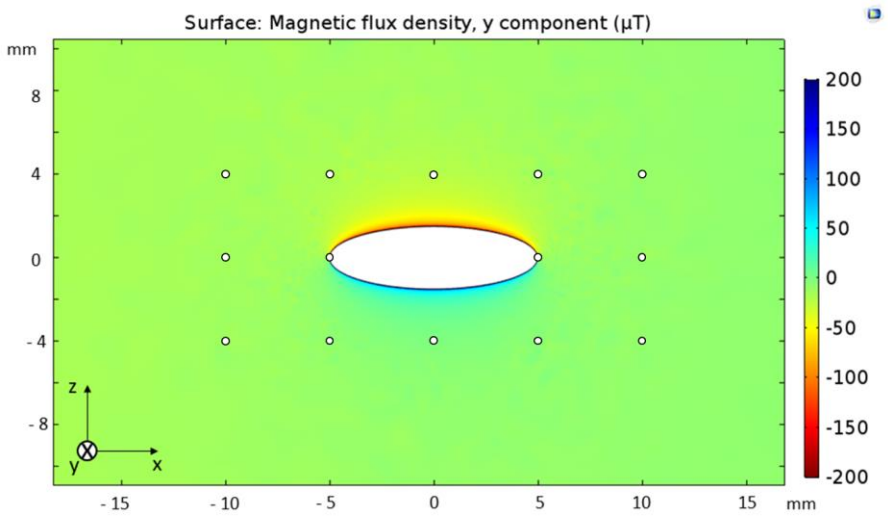

Fig. 18 FE results for B_y around the elliptical hole on the plate's surface.

4.2 Mechanical FE Model

To interpret the results from section 3.1 of this paper, the stress distribution around the elliptical hole is needed. To that end, a mechanical Finite Element model is made of the same steel plate from Fig. 1 using the software package COMSOL Multiphysics. The predefined material "Structural Steel" is used, which is linear elastic with an Elasticity Modulus of 200 GPa. The plate is constrained on the lower boundary and a force per unit area of 220 MPa is applied on the upper boundary of the plate. The plate is meshed using tetrahedral elements. The resulting von Mises stress distribution on the plate's surface around the elliptical hole is shown in Fig. 19 together with the measurement grid.

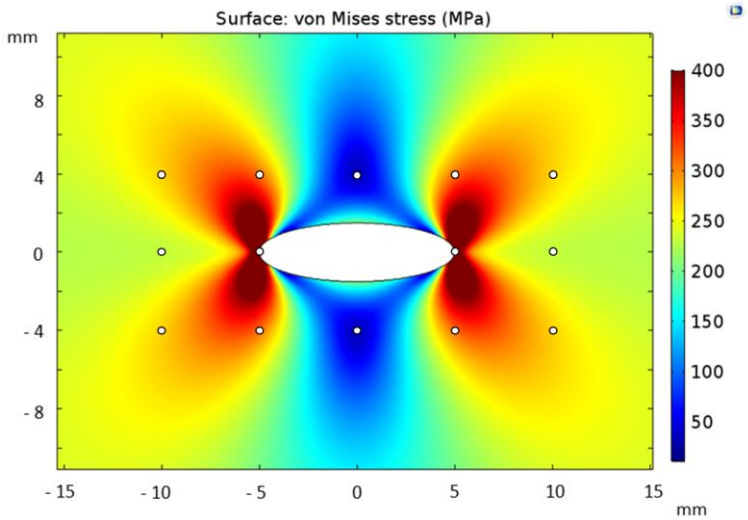

Fig. 19 FE results for von Mises stress distribution on the plate's surface.

4.3 Magnetomechanical Model

The magnetomechanical effect [7] can be implemented in the original theory of ferromagnetic hysteresis by Jiles & Atherton [13] through the effective field description H_e with the magnetostriction λ, which is defined as the strain due to an applied magnetic field. Note that this

description of the effective field is done under the assumption that the magnetostriction is very small and the applied field is in the same direction as the direction in which the stress is applied. The effective field description reads

$$H_e = H_a + \alpha M + H_\sigma, \tag{4.1}$$

where α is a field parameter representing the inter domain coupling,

and

$$H_\sigma = \frac{3}{2\mu_0}\sigma\frac{\partial\lambda}{\partial M}. \tag{4.2}$$

The same differential equation for the effective field as proposed in [13] can be applied, which reads

$$(M - M_a) = -k\delta\frac{dM}{dH_e}, \tag{4.3}$$

where k is the pinning constant and δ is a directional parameter, which takes the value 1 for increasing fields and -1 for decreasing fields. The anhysteretic M_a is a function of the effective field, which is also described in [13] and reads

$$M_a(H_e) = M_s \mathbf{L}(H_e/a), \tag{4.4}$$

where $\mathbf{L}$ is the Langevin function, $\mathbf{L}(x) = \coth(x) - 1/x$, M_s the saturation magnetization and a a constant form factor.

For a constant field H_a and varying stress, differential equation (4.3) can be rewritten, following the notation by Naus [8], as follows:

$$\frac{dM}{d\sigma} = -\frac{A_2(M,\sigma)(M - M_a)}{k\delta + A_1(M,\sigma)(M - M_a)}, \tag{4.5}$$

where

$$A_1(M,\sigma) = \frac{\partial H_e}{\partial M} = \alpha + \frac{3\sigma}{2\mu_0}\frac{\partial^2\lambda}{\partial M^2}, \tag{4.6}$$

and

$$A_2(M,\sigma) = \frac{3}{2\mu_0}\left(\frac{\partial\lambda}{\partial M} + \sigma\frac{\partial^2\lambda}{\partial M\partial\sigma}\right). \tag{4.7}$$

This differential equation can describe the magnetization for a constant field and varying stress. It is stressed in [8] that this description becomes the equivalent to the original formalism of magnetomechanics described in [7, 13, 14] for zero or constant stress. Naus also extended the model

to include the reversible contribution of the magnetization M_r. The modified differential equation for varying stress and constant field reads

$$\frac{dM}{d\sigma} = -\frac{A_2(M,\sigma)\left(M - M_a - ck\delta\frac{dM_a}{dH_e}\right)}{k\delta + A_1(M,\sigma)\left(M - M_a - ck\delta\frac{dM_a}{dH_e}\right)}, \tag{4.8}$$

where c is a constant that represents the reversible wall motion component. Following [7], the stress dependent magnetostriction is described by a double series expansion as follows:

$$\lambda(M,\sigma) = \sum_{i=0}^{\infty}\gamma_i(\sigma)M^{2i}, \tag{4.9}$$

where

$$\gamma_i(\sigma) = \gamma_i(0) + \sum_{n=1}^{\infty}\frac{\sigma^n}{n!}\gamma_i^{[n]}(0). \tag{4.10}$$

As in [7], this series is implemented up to $i=2$ and $n=1$. Following [8], $\gamma_1^{[0]} = 3\cdot10^{-18}\,A^{-2}m^2$ and all other $\gamma_i^{[n]} = 0$. The differential equation can now be written as follows:

$$\frac{dM}{d\sigma} = -\frac{\left(M - M_a - ck\delta\frac{dM_a}{dH_e}\right)\frac{3\gamma_1^{[0]}}{\mu_0}M}{k\delta + \left(M - M_a - ck\delta\frac{dM_a}{dH_e}\right)\left(\alpha + \frac{3\gamma_1^{[0]}}{\mu_0}\sigma\right)}. \tag{4.11}$$

To solve this differential equation, five hysteresis parameters are needed. These parameters are determined in [15] for several different materials by fitting the modeled hysteresis curve with a measured hysteresis curve. In the experiment described in this paper, FeE235 steel was used, which has a maximum carbon content of 0.22 mass%. Therefore, the calculated model parameters for Fe 0.2 mass% C from [15] are used to solve equation (4.11). The chosen values for the five hysteresis parameters are presented in Table 3.

Parameter	Value	Unit	Represents
M_s	$1.6\cdot10^6$	[A/m]	Saturation magnetization
a	1085	[A/m]	Form factor for the anhysteretic curve
k	320	[A/m]	Pinning constant
α	$2\cdot10^{-3}$	[-]	Inter domain coupling parameter
c	0.3	[-]	Reversible wall motion component

Table 3: Model hysteresis parameters for Fe 0.2 mass% C [15].

The effective field description described by differential equation (4.11) is solved numerically with the Euler forward method using the parameters from Table 3. The initial magnetization is chosen arbitrarily as 30% of the saturation magnetization and the applied field is chosen according to the

measured background field in Table 1 as 20 A/m. The stress is varied from zero to 235 MPa and back to zero, which is repeated two more cycles just as in the experiment. The results are presented in Fig. 20.

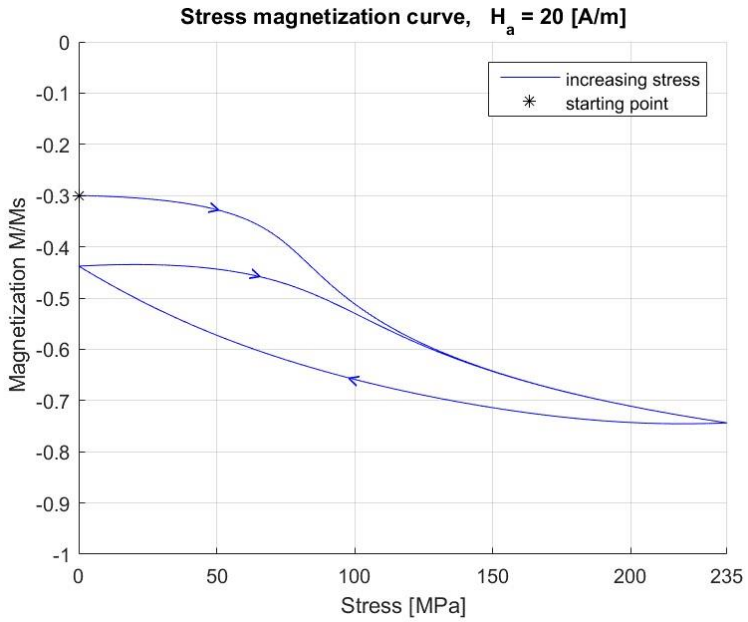

Fig. 20 Model results for the effective field description.

5. Discussion

The experimental results show a clear instantaneous magnetic response to the applied cyclic tensile load on the specimen. Equation (3.1) is used to decouple the different sources of magnetization that contribute to the measured signal. This decoupling equation is intrinsically incorrect as stress magnetization is dependent on the total magnetization of the material, see equation (4.2). Also, the stress magnetization generally has a reversible and irreversible component. The irreversible stress magnetization should be captured in the permanent magnetization, which means they are coupled as well. Nevertheless, equation (3.2) can still applied to extract the stress-induced B_y from the measurements as long as only short term effects are considered. The validity of this approach is supported by the results in Figs. 12-14 as there are no irreversible effects visible in the stress-induced magnetization curves during the three load cycles for any of the measurement points. This finding is in accordance with the work of other researchers who stated that the magnetomechanical loop tends to a stable curve after multiple cyclic loads [16], so the reversible magnetization becomes more dominant during subsequent stress cycles. Note that the specimen already experienced a few load cycles before the first magnetic measurements were taken.

The stress magnetization measurements for different locations may not be directly compared as the stress magnetization is dependent on the total magnetization, which is most likely non-uniform especially around the machined elliptical defect. Still, it can be seen that the stress magnetization at high stress concentration areas such as location (1, 2) is generally much higher than where the stress is low such as location (1, 3). For all the measurement points, the stress magnetization curves for increasing load are slightly different from those for decreasing load, but the way they differ from

each other is not consistent for each of the measurement locations, see Figs. 12-14. For most of the locations, the measured time traces show an unexpected peak when the applied load approaches zero, see Fig. 9 and Fig. 10. These peaks are most likely caused by a small overshoot of the applied load into the compressive region causing some bending stresses in the plate. This explanation is confirmed by the absence of these additional peaks for experiment 2 where the minimum loading was 3 kN in tension, see Fig. 15 and Fig. 16. Local plasticity near the elliptical hole does not seem to have a large impact on the stress magnetization for this test plate in the given environment as the results from experiment 2 in the elastic region are very similar to the results of experiment 1. The fact that each of the measurement points in experiment 2 show different values for the stress-induced magnetic flux density, supports the hypothesis that the magnetization in the plate is highly non-uniform because the stresses there are uniform.

The magnetic FE simulation in section 4.1 gives insight in the Earth-induced Magnetic Flux Leakage around the elliptical hole. A direct comparison with the measurements cannot be made because the permanent magnetization in the steel plate is unknown. The main learning from the results shown in Fig. 18 is that the spatial variation of the Earth-induced magnetic flux density is small near the measurement points, which gives more confidence in the quality of the experimental data obtained in this study. The mechanical FE simulation in section 4.2 gives insight in the distribution of stresses around the elliptical defect. Fig. 19 shows that the largest stresses are concentrated near the tips of the elliptical hole and the smallest stresses occur in the shadow areas above and underneath the elliptical hole.

Finally, the numerical simulation of the magnetomechanical effect may be used for a qualitative comparison with the experimental results. Since the magnetomechanical model describes the magnetization in the steel plate and the measurements were done at an altitude of 1 mm from the plate surface, a quantitative comparison cannot be made. Also, the permanent magnetization in the plate is unknown and the chosen values for the hysteresis parameters from Table 3 and the magnetostriction may not be accurate for this particular steel plate. Nevertheless, the numerical calculation results in a similar shape of the stress magnetization curve as the experimental results. After just one stress cycle, the calculated stress magnetization curve in Fig. 20 enters a stable loop, which corresponds with the experimental results.

6. Conclusion

The effect of the stress-induced magnetization on the SMFL near a stress concentration zone has been investigated experimentally and, as far as possible, numerically. The maximum change in measured SMFL due to applied tensile stress was approximately 25 µT near an elliptical hole in a 5 mm thick steel plate in the Earth's magnetic field. For a fatigue crack, the effect of the stress-induced magnetization may even be larger as the stress concentration factor is even higher. The measured stress-induced signal during cyclic loading showed a closed loop, so the irreversible magnetization was negligible. The expectation was that the stress-induced signals would be to some extend symmetrical around the elliptical hole as loading and geometry, and therefore stresses, are symmetrical as well. Instead, the distribution of the stress-induced magnetization appeared very irregular, which can be attributed to the inhomogeneous magnetization. From equation (4.2) it follows that the stress magnetization is dependent on the magnetization, magnetostriction and

stress. Local plasticity did not seem to have a significant effect on the stress-induced magnetization as experimental results in the elastic region showed similar magnetization curves in the same order of magnitude. A numerical simulation of the magnetomechanical effect based on a theoretical framework resulted in a similar stress magnetization curve as the ones that were measured.

For crack monitoring based on the SMFL method, the stress-induced magnetization may have a significant effect on how the measured signals should be interpreted, depending on the application. A maximum change in the SMFL of 25 μT due to stress can probably be neglected when monitoring a through thickness crack of at least 50 mm long in a thick steel plate that is part of a large structure. However, the stress-induced magnetization may be much larger near a crack front of a real fatigue crack versus at the tips of an elliptical hole. For monitoring short elliptical surface cracks, which typically have much lower magnetic flux leakage signals, the stress-induced magnetization probably has a significant effect on the measured SMFL signals near the defect. Therefore, the stress-induced magnetization should be taken into account for the interpretation of the measured signals and sizing of the crack. To this end, more research is necessary to gain better understanding of the interaction between high local stresses at a crack tip and the magnetization of ferromagnetic steel for weak background fields.

7. Acknowledgements

This work was funded by the CrackGuard Phase 2 Joint Industry Project, which is supported by Delft University of Technology, DotDotFactory, Total, Shell, ClassNK, ROSEN Group, and Feubo Feuerstein. In previous stages, this project had been supported by Delft University of Technology, DotDotFactory, Total, ClassNK, Shell, Petrobras, and ABS. The authors would also like to acknowledge Aad Vijn who wrote the code for solving the magnetomechanical model using the Euler forward method.

8. References

[1] M.P. van der Horst, M.L. Kaminski and E. Puik, Methods for Sensing and Monitoring Fatigue Cracks and Their Applicability for Marine Structures, *Proceedings of the International Offshore and Polar Engineering Conference*, Anchorage, Alaska (2013), 455-462.

[2] M.P. van der Horst and M.L. Kaminski, Slit Induced Self Magnetic Flux Leakage in a Square Steel Plate, *Proceedings of the International Offshore and Polar Engineering Conference*, Sapporo, Japan (2018), accepted.

[3] M.P. van der Horst and M.L. Kaminski, Magnetic Properties of Structural Steels for Simulation of Crack Monitoring by Finite Element Method, *Manuscript under review*.

[4] M.P. van der Horst and M.L. Kaminski, Simulation and Analysis of Earth-Induced Magnetic Flux Leakage for Monitoring Cracks in Ship and Offshore Structures, *Manuscript under review*.

[5] D.J. Craik and M.J. Wood, Magnetization changes induced by stress in a constant applied field, *Journal of Physics D: Applied Physics* **3** (1970), 1009-1016, doi 10.1088/0022-3727/3/7/303.

[6] D.L. Atherton and D.C. Jiles, Effects of stress on magnetization, *NDT International* **19** (1986), 15-19, doi 10.1016/0308-9126(86)90135-5.

[7] D.C. Jiles, Theory of the magnetomechanical effect, *Journal of Physics D: Applied Physics* **28** (1995), 1537-1546.

[8] H.W.L. Naus, Theoretical developments in magnetomechanics, *IEEE Transactions on Magnetics* **47** (2011), 2155-2162.

[9] D.C. Jiles and M.K. Devine, The law of approach as a means of modelling the magnetomechanical effect, *Journal of Magnetism and Magnetic Materials* **140-144** (1995), 1881-1882, doi 10.1016/0304-8853(94)00928-7.

[10] L. Li and D.C. Jiles, Modified Law of Approach for the Magnetomechanical Model: Application of the Rayleigh Law to Stress, *IEEE Transactions on Magnetics* **39** (2003), 3037-3039, doi 10.1109/TMAG.2003.815882.

[11] D.C. Jiles and L. Li, A new approach to modeling the magnetomechanical effect, *Journal of Applied Physics* **95** (2004), 7058-7060, doi 10.1063/1.1687200.

[12] Wuntronic, Wuntronic Tesla Meter KOSHAVA-USB n.d., http://www.wuntronic.de/en/USB-Tesla-Meter-Gauss-Meter-with-USB.html (accessed March 27, 2018).

[13] D.C. Jiles and D.L. Atherton, Theory of ferromagnetic hysteresis (invited), *Journal of Applied Physics* **55** (1984), 2115-2120, doi 10.1063/1.333582.

[14] M.J. Sablik and D.C. Jiles, Coupled Magnetoelastic Theory of Magnetic and Magnetostrictive Hysteresis, *IEEE Transactions on Magnetics* **29** (1993), 2113-2123, doi 10.1109/20.221036.

[15] D.C. Jiles, J.B. Thoelke and M.K. Devine, Numerical Determination of Hysteresis Parameters for the Modeling of Magnetic Properties Using the Theory of Ferromagnetic Hysteresis, *IEEE Transactions on Magnetics* **28** (1992), 27-35, doi 10.1109/20.119813.

[16] P. Shi, K. Jin and X. Zheng, A general nonlinear magnetomechanical model for ferromagnetic materials under a constant weak magnetic field, *Journal of Applied Physics* **119** (2016), 145103, doi 10.1063/1.4945766.